JOURNAL OF VIROLOGY, Mar. 2004, p. 2682–2692 Vol. 78, No. 6
0022-538X/04/$08.00+0 DOI: 10.1128/JVI.78.6.2682–2692.2004

Requirements for CEACAMs and Cholesterol during Murine Coronavirus Cell Entry

Edward B. Thorp and Thomas M. Gallagher*

Department of Microbiology and Immunology, Loyola University Medical Center, Maywood, Illinois 60153

Received 4 September 2003/Accepted 19 November 2003

Previous reports have documented that cholesterol supplementations increase cytopathic effects in tissue culture and also intensify in vivo pathogenicities during infection by the enveloped coronavirus murine hepatitis virus (MHV). To move toward a mechanistic understanding of these phenomena, we used growth media enriched with methyl-β-cyclodextrin or cholesterol to reduce or elevate cellular membrane sterols, respectively. Cholesterol depletions reduced plaque development 2- to 20-fold, depending on the infecting MHV strain, while supplementations increased susceptibility 2- to 10-fold. These various cholesterol levels had no effect on the binding of viral spike (S) proteins to cellular carcinoembryonic antigen-related cell adhesion molecule (CEACAM) receptors, rather they correlated directly with S-protein-mediated membrane fusion activities. We considered whether cholesterol was indirectly involved in membrane fusion by condensing CEACAMs into "lipid raft" membrane microdomains, thereby creating opportunities for simultaneous binding of multiple S proteins that subsequently cooperate in the receptor-triggered membrane fusion process. However, the vast majority of CEACAMs were solubilized by cold Triton X-100 (TX-100), indicating their absence from lipid rafts. Furthermore, engineered CEACAMs appended to glycosylphosphatidylinositol anchors partitioned with TX-100-resistant lipid rafts, but cells bearing these raft-associated CEACAMs were not hypersensitive to MHV infection. These findings argued against the importance of cholesterol-dependent CEACAM localizations into membrane microdomains for MHV entry, instead suggesting that cholesterol had a more direct role. Indeed, we found that cholesterol was required even for those rare S-mediated fusions taking place in the absence of CEACAMs. We conclude that cholesterol is an essential membrane fusion cofactor that can act with or without CEACAMs to promote MHV entry.

The infectivity of enveloped viruses often depends on the lipid composition of host cell membranes. For example, infection by certain alphaviruses, such as Semliki forest virus, requires both cholesterol and sphingolipids (38, 57, 86). Certain retroviruses and filoviruses use cholesterol-rich membrane microdomains as platforms for assembly and/or cell entry (6, 20, 31, 60). Cholesterol is an abundant and essential component of eukaryotic cell membranes. Its rigid and hydrophobic fused-ring structure preferentially associates with saturated acyl-chain lipids to form liquid-ordered microenvironments in the plasma membrane (72). These so-called lipid rafts are thought to exclude numerous integral membrane proteins while effectively concentrating others that can adopt favorable associations with the ordered, cholesterol-rich environment (11, 37, 69).

The cellular receptors for a few enveloped and nonenveloped viruses are known to reside in lipid rafts (5, 41, 62, 78). Viruses may exploit these localized cell surface proteins to facilitate rapid multivalent interactions with the host cell. The ensuing high-avidity binding and positive cooperativity may promote productive virus entry (18, 83). Raft-like environments may also serve as portals for virus entry into distinct intracellular organelles; for example, the caveolar endocytosis of simian virus 40 precedes its transport into the endoplasmic reticulum lumen (61). Finally, during enveloped virus entry, the lipid components of these rafts may participate directly during coalescence with the virion membrane. For example, cholesterol has a role in promoting and stabilizing the local bilayer bending that takes place during membrane fusion (16, 27, 32, 66). Indeed, the composition of opposing lipid bilayers can generally determine whether protein-mediated membrane fusion is successfully completed, as evidenced by the behavior of lipids, such as lysophosphatidylcholines, which arrest enveloped virus entry at intermediate states where opposing membranes remain unmixed yet tethered by the two ends of a single polypeptide (30, 51).

Changes in the lipid composition of cellular membranes can have pronounced effects on the outcome of coronavirus infection. This was first documented in tissue culture, where the syncytia expanding from foci of murine hepatitis virus (MHV) infection were substantially larger after cholesterol supplementations (13, 19, 67). Subsequent in vivo experiments established correlations between cholesterol-rich diets and susceptibility of mice to pathogenic MHV infection (9). We have been intrigued by these observations, in part because our ongoing studies have revealed considerable variability in the efficiency of MHV-induced membrane fusion (42). Such variability has often been unrelated to the abundance of carcinoembryonic antigen-related cell adhesion molecules (CEACAMs) on host cells, a cellular receptor for MHV (22, 87, 88). With the hypothesis that these variabilities arise because MHV-induced membrane fusion (and consequent syncytial development) requires specific lipid cofactors in addition to CEACAM receptors, we sought to understand how cholesterol augments MHV entry.

* Corresponding author. Mailing address: Department of Microbiology and Immunology, Loyola University Medical Center, 2160 S. First Ave., Maywood, IL 60153. Phone: (708) 216-4850. Fax: (708) 216-9574. E-mail: tgallag@lumc.edu.

MATERIALS AND METHODS

Cells and viruses. All cell lines were propagated as adherent monolayer cultures. HeLa-tTA (tTA denotes tetracycline-controlled transactivator) (29), sac- cells (82), rabbit kidney clone 13 cells, and baby hamster kidney (BHK) cells were grown in Dulbecco's modified Eagle medium (DMEM) supplemented with 10% heat-inactivated fetal bovine serum (ΔFBS) (Atlas Biologicals, Fort Collins, Colo.) (DMEM–10% ΔFBS). HeLa-tTA-CEACAM (isoform 1a, line 3) (63) cells were cultured in DMEM–10% ΔFBS containing 2.5 μg of mycophenolic acid per ml, 250 μg of xanthine per ml, 20 μg of hypoxanthine per ml, and 100 μg of G418 per ml. HeLa-tTA $CEACAM_{TM}$ and HeLa-tTA $CEACAM_{GPI}$ cells (pTRE2hyg stable transfectants as described below) were cultured in DMEM–10% ΔFBS containing 100 μg of G418 per ml and 100 μg of hygromycin B per ml. Murine 17 cl 1 fibroblasts (80) were grown in DMEM containing 5% tryptose phosphate broth (Difco Laboratories) and 5% ΔFBS. DBT (murine astrocytoma) cells (35) were grown in minimal essential medium containing 10% tryptose phosphate broth and 5% ΔFBS. Soluble-receptor-secreting 293 EBNA-N-$CEACAM_{Fc}$ ($sMHVR_{Fc}$) cells (26) were grown in DMEM–10% ΔFBS containing antibiotics G418 (100 μg/ml) and hygromycin B (200 μg/ml). All growth media were buffered with 0.01 M sodium HEPES (pH 7.4).

Coronavirus strains JHM (prototype strain MHV-4) (85), JHM-X (48), and A59 (68) were plaque purified three times on HeLa-CEACAM cells and subsequently propagated after a 1-h adsorption on 17 cl 1 cells at a low-multiplicity infection (0.01 PFU/cell) in serum-free medium (SFM) with 0.01% (wt/vol) bovine serum albumin (BSA). Inocula were replaced with growth medium containing 2% ΔFBS, and the cell supernatant was harvested at 18 hours postinfection (hpi), followed by clarification of medium by differential centrifugation to remove cellular debris (sequential spins of 15 min at 2,000 × *g*, followed by 30 min at 10,000 × *g*). Infectivity was determined by plaque assay, using either HeLa-CEACAM or 17 cl 1 as indicator cells in DMEM–1% ΔFBS and 0.5% (wt/vol) Noble agar (Difco). Vaccinia virus recombinants, each harboring spike cDNA of a particular coronavirus strain, were generated and propagated in rabbit kidney clone 13 cells as previously described (42). Vesicular stomatitis virus (VSV) was propagated in BHK cells after a low-multiplicity infection and collected from cells after the first signs of cytopathic effect. VSV was clarified as described above for MHV by differential centrifugation, prior to application onto cell monolayers.

Infectivity determinations after cholesterol extractions and supplementations of cells. *methyl*-β-Cyclodextrin (MβCD) (Sigma catalog no. C-4555) or cholesterol-MβCD inclusion complexes (Sigma catalog no. C-4951) were serially diluted in serum-free DMEM (SFM), and 1-ml volumes were applied to 10^6 adherent cells in 10-cm^2 dishes at ~70 to 80% confluency for 30 min at 37°C (40, 73). Cells were then rinsed three times with 2 ml of phosphate-buffered saline (PBS) to remove residual membrane-impermeant MβCD (1, 59). Total cell cholesterol contents before and after cholesterol depletions were measured from cell lysates using the Amplex red cholesterol assay from Molecular Probes, which detects the hydrogen peroxide product of a cholesterol oxidase enzyme reaction (4). Following cholesterol extractions, SFM containing serial dilutions of MHV or VSV were then applied to cells for 1 h at 37°C, followed by an additional three rinses with PBS. Cells were prepared for plaque development, and plaques were enumerated 2 to 3 days later after the cells were fixed with formalin and stained with crystal violet in saline and ethanol. Alternatively, MβCD was applied to cells from 2.5 to 3 hpi after rinsing off adsorbed virus inocula. The cells were then processed for plaque assay.

Virion-cell binding. HeLa-CEACAM cells were exposed to MβCD or cholesterol-MβCD as described above, rinsed three times with ice-cold PBS, chilled to 4°C, and overlaid with radiolabeled MHV. Virus was metabolically labeled from ~12 to 15 hpi (after starving the cells in cysteine- and methionine-free medium) in MHV (A59)-infected 17 cl 1 cells cultured in SFM with 1% dialyzed ΔFBS containing 100 μCi of [^{35}S]Cys/Met Translabel (ICN). ^{35}S-labeled MHV A59 was harvested from the above infected cell cultures and placed over 30 and 50% (wt/wt) sucrose layers in HNB (50 mM HEPES, 100 mM NaCl, 0.01% [wt/vol] BSA [pH 7.4]). Virions were subjected to ultracentrifugation in a Beckman SW41 rotor and collected from the 30/50% sucrose interface as described before (25). Radiolabeled virions were subsequently concentrated by pelleting through 30% sucrose, and pellets were resuspended in SFM. ^{35}S-labeled MHV A59 (5×10^5 cpm) in 1 ml of SFM containing 0.01% BSA was applied to cyclodextrin (CD)-treated or untreated HeLa-CEACAM or HeLa-$CEACAM_{GPI}$ cells, incubated to equilibrium (2 h at 4°C), and then removed. Cells were rinsed three times with ice-cold PBS and dissolved with PBS containing 0.5% Nonidet P-40 (NP-40), and radioactivity associated with the lysates and media was quantified by scintillation counting to determine the percentage of cell-associated MHV.

Qualitative and quantitative fusion assays after cholesterol treatments. Microscopic inspection of MHV-induced syncytia after cholesterol treatments was performed after cultivating cells for ~1 h with cellular fluorescent probe Cell Tracker green CMFDA (5-chloromethylfluorescein diacetate) at 2 μM in SFM or octadecylrhodamine (R18) at 2 μg/ml in SFM, per Molecular Probes. Unincorporated CMFDA and R18 were rinsed away from cells prior to CD treatments. Alternatively, CEACAM-independent cell-cell fusion was visualized through a variation of the cell fusion-dependent reporter gene activation assay of Nussbaum et al. (58). Target HeLa cells were transiently treated with Lipofectamine (Invitrogen) with the reporter gene pTM3-eGFP for T7 RNA polymerase-driven expression of enhanced green fluorescent protein (eGFP) (14, 54). After transfection, target cells were treated with MβCD for 30 min, rinsed, and placed over spike-bearing effector cells that had previously been infected with vTF7.3 (T7 RNA polymerase) (24) and vTM1-S_{JHM} (26) (as also described below). Photomicrographs were taken after effector-target cell-cell fusion and subsequent intercellular transfer of T7 RNA polymerase and T7-driven expression of eGFP. Images were captured by using Magna Fire software with a Leica DM-IRB inverted microscope fitted with an Optronics charge-coupled device camera. Reporter gene activation of eGFP was not effected by MβCD treatments of cells that had previously been transfected with pTM3-eGFP and subsequently infected with vTF7.3. Cholesterol extractions after MβCD treatment were monitored in parallel after previously cultivating cells overnight in tritium cholesterol ([1,2-^{3}H(N)]-cholesterol; Perkin-Elmer Life Sciences catalog no. NET-139) and measuring cell- and clarified-medium-associated radioactivity with a Beckman scintillation counter.

The cell fusion-dependent reporter gene (β-galactosidase) activation assay of Nussbaum et al. (58) was adapted for quantitative studies of spike-mediated membrane fusion. To measure virion-mediated intercellular fusion (fusion from without) (25), parallel HeLa-CEACAM cultures were infected separately with vTF7.3 and vCB21R-lacZ (T7-driven β-galactosidase) (3), each at 2 PFU per cell. Six hours later, both cultures were exposed to graded doses of MβCD and then rinsed as described above. Cells from both cultures were removed from the wells with trypsin, diluted in DMEM with FBS, and then mixed together. Cocultures were centrifuged at 500 × *g*, and cells were resuspended to 10^6 cells/ml in 17 cl 1 medium containing MHV A59 (multiplicity of infection [MOI] of ~10 to 100 PFU per cell) and immediately repelleted and added back to tissue culture wells (5×10^5 cells per 5-cm^2 well). At hourly intervals, media were removed from these wells, and cells were lysed with PBS containing 0.5% NP-40. β-Galactosidase was quantified in each lysate using a colorimetric assay measuring turnover of chlorophenyl red β-galactopyranoside (CPRG) at an optical density of 590 nm. Reporter gene activation of β-galactosidase was not effected by MβCD treatments of cells that had previously been coinfected with both vTF7.3 and vCBR21R-lacZ.

To quantify S-mediated cell-cell fusion (spike protein from cDNA clones), effector (spike-bearing) cells were generated by coinfection with vTF7.3 and vTM1-$S_{JHM\text{-}X}$ (26), each at 2 PFU per cell. Target cells (either HeLa, HeLa-CEACAM, or HeLa-$CEACAM_{GPI}$) were coinfected with vaccinia virus WR and vCB21R-lacZ, each at 2 PFU per cell. At 6.5 hpi, target cells were exposed to graded MβCD doses as described above. Target cells were subsequently washed in PBS, trypsinized, rinsed in DMEM–10% ΔFBS, pelleted, resuspended in SFM, and then placed over effector cells at a 1:1 ratio. Cell lysates were subsequently measured for β-galactosidase as described above.

Preparation, isolation, and assessment of TX-100-insoluble membranes. To evaluate the buoyant densities of CEACAMs after nonionic detergent extractions, uninfected HeLa-CEACAM or -$CEACAM_{GPI}$ cells were rinsed with ice-cold PBS and chilled to 4°C. To ~10^7 adherent cells, 1 ml of cold TNE (50 mM Tris-HCl [pH 7.4], 100 mM NaCl, 1 mM EDTA) containing 0.2 or 1% (vol/vol) Triton X-100 (TX-100) was added and kept at 4°C for 30 min. Cell extracts were passed five times through a 27-gauge needle and subsequently pelleted (700 × *g* for 5 min). Postnuclear supernatants were mixed with equal volumes of 80% (wt/vol) sucrose in TNE containing 0.2 or 1.0% TX-100 and protease inhibitors (Sigma protease inhibitor cocktail P2714). Samples were placed in ultracentrifuge tubes and overlaid sequentially with 7 ml of 38 or 30% (wt/vol) and 2.5 ml of 5% (wt/vol) sucrose in TNE (70). Following centrifugation at 4°C for 18 h at 285,000 × *g* in a Beckman SW41 rotor, 1.3-ml fractions were collected from the air-gradient interface, and aliquots were mixed with solubilizing buffer (63 mM Tris-HCl [pH 6.8], 2% [wt/vol] sodium dodecyl sulfate [SDS], 2.5% [wt/vol] Ficoll, 0.0025% [wt/vol] bromophenol blue, 5% [vol/vol] 2-mercaptoethanol [final concentrations given]), heated at 100°C for 5 min, and processed for SDS-polyacrylamide gel electrophoresis and immunoblotting (44). CEACAMs were detected using recently generated rabbit antiserum raised against purified N-$CEACAM_{Fc}$ from 293 EBNA-N-$CEACAM_{Fc}$-secreting cells. Western immuno-

blotting was performed as described previously (65) and quantified using Scion software (Scion Corporation).

To assess the solubilization and fractionation of cell membranes during preparation of detergent-resistant membranes (DRMs), the transferrin receptor and ganglioside GM1 standards were assayed in parallel to probes for CEACAMs (33). Transferrin receptor was detected by immunoblotting with anti-human transferrin receptor (clone H68.4) (catalog no. 13-6800, Zymed Laboratories, Inc.) and then with alkaline phosphatase-conjugated, affinity-purified goat antibody to human immunoglobulin G (IgG) Fc (Cappel catalog no. 59289). Ganglioside GM1 was detected after dot blotting with cholera toxin-peroxidase (Sigma) and tetramethylbenzidine-stabilized substrate for horseradish peroxidase from Promega (catalog no. W4121). To measure the cholesterol content in DRM fractions, cells were labeled with [1,2-^{3}H(N)]cholesterol overnight prior to DRM extraction. The total cholesterol content in each sucrose gradient fraction was quantified by scintillation counting.

In assays designed to specifically detect only those CEACAMs on the plasma membrane, HeLa-CEACAM$_{TM}$ or HeLa-CEACAM$_{GPI}$ cells were overlaid with ^{35}S-labeled S1 (45) for 2 h at 4°C, washed with PBS, extracted with TNE containing TX-100, and fractionated as described above. The amounts of ^{35}S-labeled S1 in sucrose gradient fractions were determined by scintillation counting. Alternatively, cell surface-associated CEACAMs were detected after surface biotinylation with NHS-LC-biotin from Pierce (catalog no. 21335). Cells were suspended in a minimal volume of PBS (pH 8.0), biotinylated (1 mg/ml biotin) at 4°C for 20 min, and rinsed three times in cold 50 mM Tris-containing buffer at a pH of 8.0 to quench unreacted biotin. Cells were subsequently rinsed with ice-cold PBS and subjected to TX-100 extraction and fractionation as mentioned above. Biotinylated proteins were captured with streptavidin-agarose beads and processed for immunoblotting as described above.

Engineering GPI-anchored CEACAMs and initial characterizations of CEACAM$_{GPI}$-bearing cells. The open reading frame of the extracellular CEACAM1a ectodomain was fused upstream of the glycosylphosphatidylinositol (GPI)-coding signal sequence of human carcinoembryonic antigen (CEA) to create the chimera CEACAM$_{GPI}$ (21, 71). The CEA-GPI cleavage or attachment (omega) site was amplified from CEA (American Type Culture Collection catalog no. 587150, GenBank accession no. M17303) with an upstream oligodeoxyribonucleotide encoding part of CEACAMecto fused in frame to the GPI-encoding region of CEA as indicated: 5′ C TCA GAT-AGC ATC ACA GTC TCT GCA TCT GG (the hyphen demarcates the junction between CEACAM and CEA-GPI). The resultant CEA-GPI PCR fragment was fused to CEACAMecto via overlap extension PCR (36), and the intended CEACAMecto-CEA$_{GPI}$ junction was confirmed after sequencing on an ABI Prism 3100 genetic analyzer. Transmembrane (TM)-anchored CEACAMs were amplified in parallel, and constructs were shuttled into pTRE2hyg from Clontech. HeLa-tTa cells (G418 resistant) were treated with Lipofectamine with either pTRE2hyg-CEACAM$_{TM}$ or pTRE2hyg-CEACAM$_{GPI}$, and stable G418- and hygromycin B-resistant clones were isolated via limiting dilutions and fluorescence-activated cell sorting on a FACStar Plus. Mean fluorescent intensities of cell surface CEACAMs were measured by indirect immunofluorescence flow cytometry of trypsinized cells on a FACS Calibur using rabbit antisera to N-CEACAM-Fc and fluorescein-conjugated goat IgG directed against rabbit IgG (Cappel catalog no. 55646). The presence of GPI anchors was authenticated as described elsewhere (71) by incubating CEACAM$_{GPI}$-bearing cells with phosphatidylinositol-specific phospholipase C (PI-PLC) (Sigma catalog no. P-5542) and detecting cell-liberated CEACAM ectodomains via immunoblotting with anti-N-CEACAM-Fc from a 10-fold concentrate of cell supernatants (concentrated via an Amicon Centricon filtration device with a molecular size cutoff of 30 kDa). HeLa CEACAM$_{TM}$ (clone CM5) and HeLa CEACAM$_{GPI}$ (clone GM3) displayed similar cell surface CEACAM mean fluorescent intensities by flow cytometry and were assessed in parallel to measure susceptibilities to MHV infection and membrane fusion.

RESULTS

Cholesterol levels can determine cellular susceptibility to MHV infection. Numerous studies have demonstrated that cell cultures exposed to MβCD, a well-studied cyclic polysaccharide that specifically chelates cholesterol (39), become resistant to infection by a variety of enveloped viruses (7, 49). That MHV infection might also be sensitive to MβCD was suggested by the results of previous studies indicating that cholesterol-supplemented murine cells were hypersensitive to MHV-induced syncytia (13, 19). Thus, we exposed murine 17 cl 1 fibroblast monolayers to increasing doses of MβCD for 30 min at 37°C. At the highest concentration (20 mM), this MβCD exposure removed ~40% of total cell cholesterol, as determined by the Amplex red cholesterol assay (4). This treatment had no deleterious effect on cell growth rate, adherence, or permeability to trypan blue (data not shown). Exposure to MβCD immediately prior to MHV inoculation had a suppressive effect on plaque development (Fig. 1A). By contrast, the same MβCD exposures after viral adsorption (2.5 to 3 hpi) had no effect, indicating that the drug treatments did not irreversibly arrest the replicative events occurring during the eclipse phase. Infections by cholesterol-independent VSV were unaffected by the MβCD treatments (Fig. 1A). We also supplemented cholesterol in 17 cl 1 cells by applying CD-solubilized cholesterol (10 to 100 μg/ml) for the 30 min immediately prior to MHV inoculation. This treatment resulted in increases in the plaque number of 2- to nearly 10-fold; the plaques were also distinguished by their larger size and clear centers (Fig. 1B). Thus, it is likely that cholesterol acts as an MHV entry cofactor, and it is also likely that the MβCD-induced resistance to MHV infection results from the absence of cholesterol per se, not from hypothetical indirect effects of the cholesterol extraction process (Fig. 1A). These general cholesterol-dependent effects on MHV infection were also observed in the murine cell lines DBT, sac-, and the human HeLa-CEACAM line.

Sensitivity to cholesterol extraction varied moderately with virus strain. Strain A59-derived plaques developed even at high MβCD doses (Fig. 1C). We attributed these plaque developments to the long-term maintenance of the inoculated particles on cell surfaces, which presumably generated infections once the MβCD-treated cells repleted their membrane cholesterol via endogenous sterol synthesis pathways. Consistent with this notion, we found that residual A59 infectivity was eliminated by incubation with proteinase K, which removes cell surface viruses (data not shown). The more MβCD-sensitive MHV-JHM likely lacked this cell surface stability. Indeed, JHM is a well-known thermolabile strain that rapidly loses infectivity at physiologic pH and temperature (42, 79), particularly when associated with CEACAM receptors (50).

Extraction of cholesterol from target cells blocks MHV-induced membrane fusion. That cholesterol levels specifically influence MHV entry at the virus-cell membrane fusion stage was tested using quantitative virus-receptor binding and virus-cell fusion assays (25). In these assays, we used MHV A59, a thermostable strain with robust growth characteristics (82) and HeLa-CEACAM cells, stable transfectants that display up to 300,000 CEACAMs per cell (64). Exposing these cells to MβCD or cholesterol-MβCD complexes did not change their capacity to bind ^{35}S-labeled A59 particles (Fig. 2), nor did the treatments alter cellular morphology or cell-cell contacts (Fig. 3A). However, A59-induced intercellular fusions were arrested by MβCD and enhanced by cholesterol (Fig. 3). Thus, the CEACAM-bound A59 virions could not develop intercellular fusion pores after cholesterol depletion from the target cell plasma membranes.

Distribution of CEACAMs after cells were treated with cold TX-100. Our data suggested that MHV entry required that both CEACAMs and cholesterol cluster together in plasma membranes, so we looked at whether CEACAM receptors

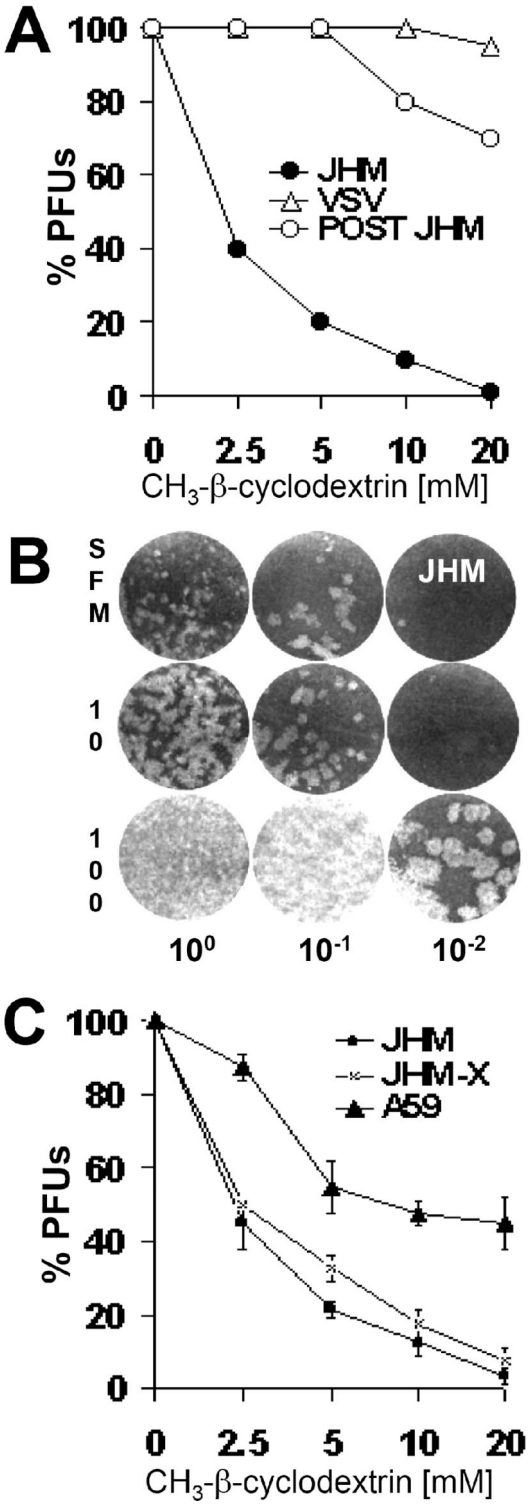

FIG. 1. Quantification of virus titer on cells pretreated with MβCD or cholesterol-MβCD inclusion complexes. 17 cl 1 cell monolayers were incubated in SFM with the indicated doses of MβCD (A and C) or cholesterol-MβCD complexes (in micrograms per milliliter) (B) for 30 min at 37°C. Cells were subsequently rinsed and overlaid with serial dilutions of the MHV strain JHM, JHM-X, or A59 or with VSV. In one experiment shown in panel A, MβCD was added after JHM adsorption for 30 min. The number of PFU was determined after 3 days. Error bars represent the standard deviations of the means for two independent determinations.

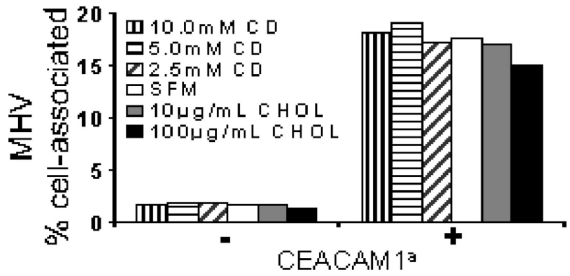

FIG. 2. MHV-cell binding after cholesterol extraction or supplementation. HeLa (−) and HeLa-CEACAM (+) cells were cultured in SFM with the indicated doses of MβCD (CD) or cholesterol-MβCD (CHOL) complexes for 30 min at 37°C. Cells were subsequently rinsed and incubated at 4°C for 2 h with ^{35}S-labeled MHV strain A59 (~5×10^5 cpm). Unadsorbed virions were rinsed away, and cell-associated radioactivity was calculated as a percentage of the total ^{35}S-labeled virus added.

might colocalize with cholesterol-rich membrane microdomains in susceptible cells. While the integral-membrane CEACAMs have no obvious features that might suggest their concentration into cholesterol-rich membranes (52), cell adhesion molecules are often found localized in lipid rafts (53, 56). Membrane microdomains enriched in cholesterol and sphingolipid are distinguished by their resistance to solubilization in cold TX-100. These TX-100 DRMs are readily separated in sucrose gradients from the much larger fraction of detergent-soluble cellular material by virtue of their low lipid densities (11).

By the criteria of 1% TX-100 insolubility and low density in sucrose gradients, CEACAMs were not raft associated (Fig. 4). To determine whether DRMs were in fact isolated, we detected ganglioside GM1 in gradient fractions using a cholera toxin-peroxidase conjugate. Greater than 70% of GM1 was in raft fraction 3. By contrast, the raft-excluded transferrin receptor remained in fractions 9 to 11, completely solubilized and at the bottom of the gradient.

To address the possibility that our lysis conditions disrupted weak interactions between DRMs and CEACAMs, we reduced TX-100 concentrations to 0.2%, a concentration often used to prepare DRMs from various cell lines (28). Under these more gentle conditions, we did isolate DRMs harboring small amounts (~10%) of the CEACAMs (Fig. 5A, top blot). Through cholesterol supplementation or depletion, the relative proportion of these DRM-associated CEACAMs could be predictably varied. Supplementations with cholesterol-rich media increased the proportion of low-density (lipid-associated) CEACAMs to ~20%, while depletions through MβCD extraction effected solubilization (Fig. 5A, CHOL and CD blots).

To determine whether the Western blot signals reflected the proportion of cell surface CEACAMs, we incubated HeLa-CEACAM cells with ^{35}S-labeled S1, the receptor-binding subunit of MHV (43), then lysed the cells with our low concentration of 0.2% TX-100, and fractionated the cellular material on gradients. About 10% of the ^{35}S-labeled S1 was found in DRM fractions 3 to 6 (Fig. 5B), consistent with the distribution of CEACAMs determined by Western blotting. These fractions contained about 30% of total cellular cholesterol, as measured by the distribution of [^{3}H]cholesterol in radiolabeled cells (Fig. 5B).

Using the results when 0.2% TX-100-resistant membranes were fractionated, we began to identify relationships between

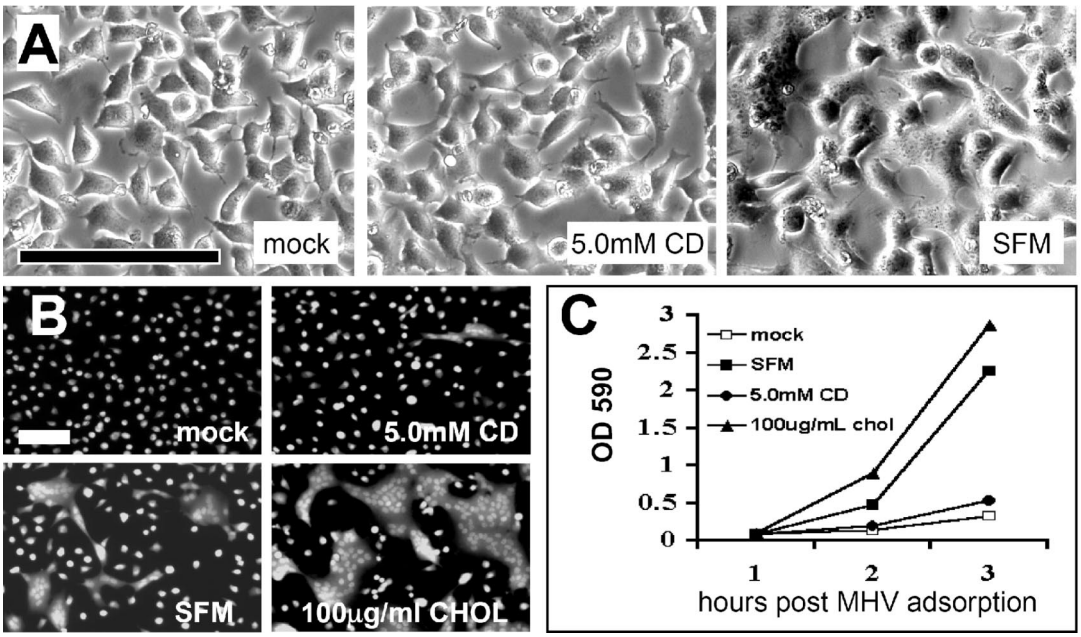

FIG. 3. Microscopic depictions (A and B) and quantification (C) of MHV-induced syncytia after cholesterol enrichment or depletion. (A and B) HeLa-CEACAM cells were incubated in SFM containing the indicated concentrations of MβCD (CD) or cholesterol (CHOL) for 30 min at 37°C, rinsed with PBS, incubated for 3 h with MHV strain A59 (MOI, ~10), and then photographed using phase-contrast (A) or fluorescence (B) microscopy. In panel B, cells were labeled with the fluorescent cytosolic dye CMFDA. Bars, 200 μm. (C) The indicated doses of CD and cholesterol (chol) were incubated with HeLa-CEACAM cells that had been prepared for cell fusion-dependent reporter gene activation, as described in Materials and Methods. Cells were rinsed with PBS, A59 virions were applied (MOI, ~10), and reporter gene product β-galactosidase enzyme activities in lysates were quantified by measuring CPRG substrate turnover at an optical density of 590 nm (OD 590).

the abundance of DRM-associated CEACAMs and cellular susceptibility to MHV infection (Fig. 5C). However, in these HeLa-CEACAM cell cultures, cholesterol only modestly increased susceptibility to MHV infection. The results of Fig. 5C represent an extreme case in which the supplementations affected a threefold increase in plaque number.

Relocalizing CEACAMs into DRMs does not increase susceptibility to MHV infection. Results depicted in Fig. 5 suggested that the CEACAMs in cholesterol-rich DRMs might serve as preferred sites for MHV entry. If this were true, then cells with clustered, DRM-associated CEACAMs might exhibit hypersensitivity to MHV infection. We sought to create this type of CEACAM localization by replacing the CEACAM transmembrane and cytoplasmic tail (TM/CYTO) region with sequences specifying posttranslational addition of GPI. The GPI moiety has a well-known predilection for cholesterol-rich DRMs (10), and this strategy to relocalize viral receptors on plasma membranes has been used to determine whether human immunodeficiency viruses might enter through DRMs (20). In addition, several human CEACAMs are in fact GPI anchored (74), making it likely that GPI-anchored murine CEACAM1a would support MHV entry and have potential relevance to understanding entry of human coronaviruses in cells (55).

To generate $CEACAM_{GPI}$, cDNA encoding the CEACAM1a ectodomain was fused to the portion of human CEA cDNA encoding those residues specifying the addition of GPI (Fig. 6A). Plasmid DNAs encoding either TM- or GPI-anchored forms were treated with Lipofectamine, overlaid on HeLa cells, and drug-resistant clones were isolated. To assess cDNA expression, several clones were incubated with anti-CEACAM antibodies and subjected to flow cytometry. TM and GPI clones with equivalent CEACAM levels were selected for subsequent comparative analyses (Fig. 6B). In an effort to more closely represent physiologic conditions, we chose to focus on cell lines whose CEACAM levels were substantially lower (~10-fold lower [fluorescence-activated cell sorting data not shown]) than the HeLa-CEACAM line used in our previous experiments (Fig. 2 to 5). Using these selected clones, we then

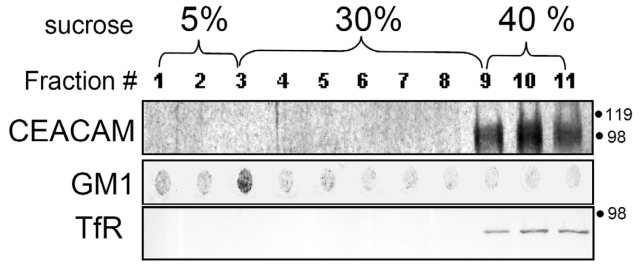

FIG. 4. Distribution of CEACAMs after cell fractionation in 1% TX-100-containing sucrose gradients. HeLa-CEACAM cells were chilled to 4°C and dissolved in 1% TX-100. Postnuclear supernatants were adjusted to 40% sucrose and layered underneath 30 and 5% sucrose. Samples were spun to equilibrium, and CEACAMs in gradient fractions were detected by Western immunoblotting using CEACAM antiserum. The positions of the molecular mass markers (in kilodaltons) are indicated to the right of the blot. The distributions of ganglioside GM1 and transferrin receptor were identified using cholera toxin-peroxidase and antitransferrin antibodies, respectively. TfR, transferrin receptor.

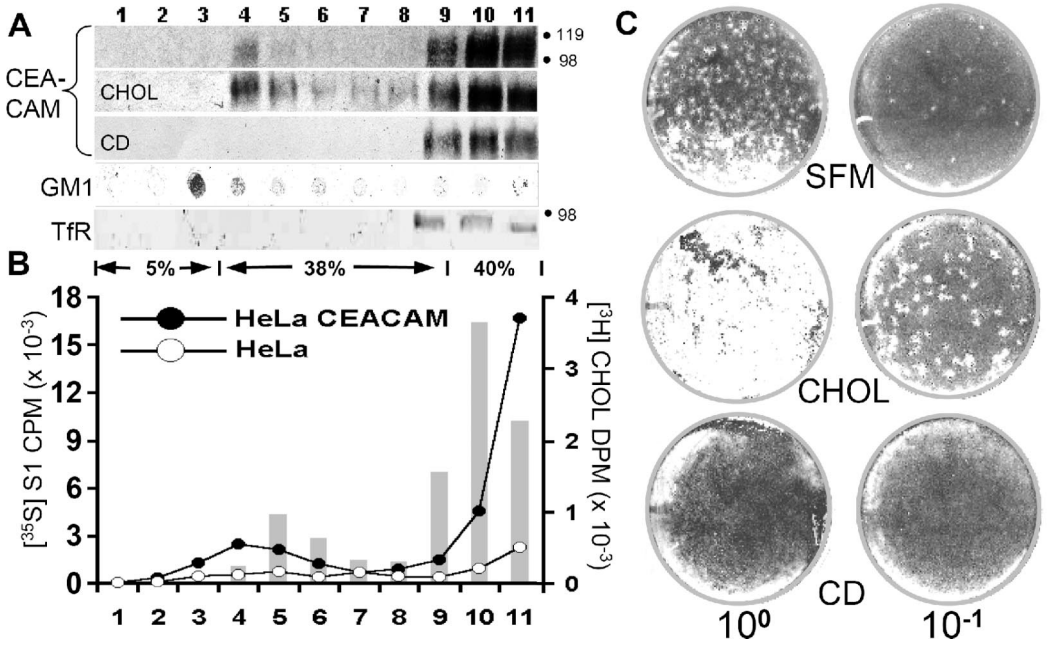

FIG. 5. Distribution of CEACAMs in 0.2% TX-100-containing sucrose gradients after cholesterol enrichment or depletion. (A) CEACAM distributions were determined as described in the legend to Fig. 4, except that prior to addition of detergent, cell monolayers were cultured for 30 min with either 100 μg of cholesterol (CHOL) per ml or 10 mM CD, as indicated. The positions of molecular mass markers (in kilodaltons) are indicated to the right of the blot. TfR, transferrin receptor. (B) To identify cell surface CEACAMs in flotation gradients, ^{35}S-labeled S1 was bound to cells prior to detergent extraction and processing as described above. In parallel, cells labeled overnight with [^{3}H]cholesterol were chilled and processed as described above to determine the distribution of cholesterol in gradient fractions. ^{35}S-labeled S1-specific and [^{3}H]cholesterol radioactivity was determined by scintillation counting (counts shown as 10^3 cpm or 10^3 disintegrations per minute [DPM]). (C) HeLa CEACAM cells were cultured for 30 min in SFM alone or in SFM supplemented with 100 μg of cholesterol (CHOL) per ml or 10 mM CD, rinsed, and then infected with MHV-JHM. Plaques were stained with crystal violet 3 days postinfection.

added ^{35}S-labeled MHV, as described previously (Fig. 2), to measure virus-binding capacities. HeLa cell clones with equivalent CEACAM surface levels, as determined by flow cytometry, bound equivalent amounts of ^{35}S-labeled MHV particles (Fig. 6C, hatched bars), indicating that the membrane-tethering structure (TM protein or GPI lipid) had no measurable effect on the abilities of CEACAMs to bind viruses. Next, to confirm the existence of the GPI anchor, clones were incubated with PI-PLC prior to the addition of ^{35}S-labeled MHV. PI-PLC treatments specifically reduced MHV binding to HeLa-CEACAM$_{GPI}$ cells (Fig. 6C). This finding was in accordance with PLC-mediated release of CEACAMs specifically from the HeLa-CEACAM$_{GPI}$ cells, as evidenced by the presence of soluble receptor ectodomains in media (Fig. 6C).

Using these characterized HeLa cell clones, cell surface proteins were biotinylated, 1% TX-100 extracts were prepared,

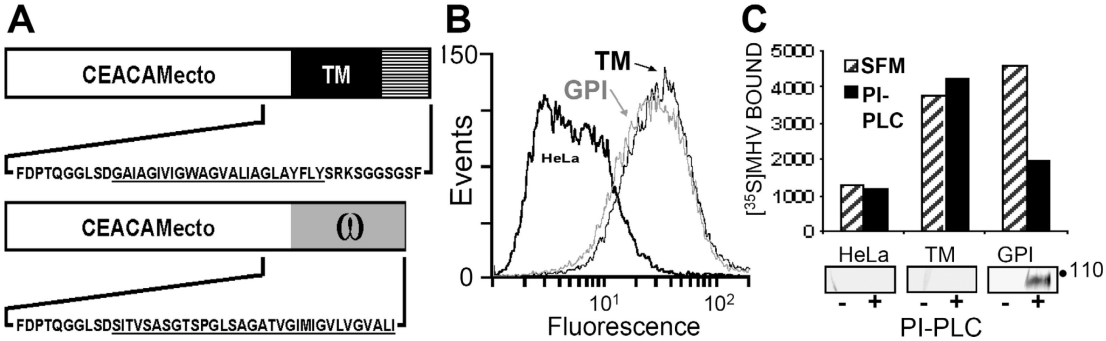

FIG. 6. Construction and characterization of HeLa-CEACAM$_{GPI}$ cells. (A) Linear depiction of CEACAM$_{TM}$ and CEACAM$_{GPI}$. The predicted TM span sequence is underlined, as is the signal peptide containing the omega sequences conferring en bloc attachment of GPI lipid. The carboxy-terminal sequences of the constructs were determined as indicated. (B) Surface fluorescence intensities of HeLa-CEACAM$_{TM}$ (TM) and HeLa-CEACAM$_{GPI}$ (GPI) cells. Flow cytometry profiles of cell surface CEACAMs were determined by indirect immunofluorescence using CEACAM antiserum. (C) Quantification of ^{35}S-labeled MHV binding to HeLa cells lacking CEACAMs and to HeLa cells bearing TM- and GPI-anchored CEACAMs. Binding assays were additionally performed after the cells were treated with PI-PLC. The blots at the bottom of panel C depict CEACAMs in media after the cells were incubated with PI-PLC (+). The position of the 110-kilodalton molecular mass marker is indicated to the right of the GPI blot.

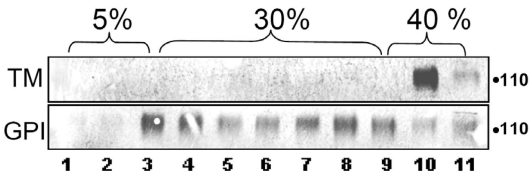

FIG. 7. Distribution of cell surface $CEACAM_{GPI}$ in 1% TX-100-containing sucrose gradients. Cell surface proteins were biotinylated, and cells were then treated with cold 1% TX-100. Extracts were fractionated in sucrose gradients, biotinylated proteins were captured from gradient fractions with streptavidin-agarose, and TM- and GPI-anchored CEACAMs were visualized by immunoblotting after SDS-polyacrylamide gel electrophoresis. The position of the 110-kilodalton molecular mass marker is indicated to the right of the blot.

and the distribution of plasma membrane- and DRM-associated CEACAMs was determined by immunoblotting of sucrose gradient fractions (Fig. 7). As predicted, $CEACAM_{GPI}$ was largely detergent insoluble (~70% in low-density fractions 3 to 9), while $CEACAM_{TM}$ was entirely soluble (100% in fractions 10 and 11). This pattern of $CEACAM_{GPI}$ distribution was similar to that observed in previous studies in which other proteins were appended to GPI and monitored for their TX-100 insolubilities (5, 17). Using the method of ^{35}S-labeled S1 complexing prior to DRM preparation (Fig. 5B), we confirmed that these Western immunoblot profiles reflected the distribution of CEACAMs capable of virus binding (data not shown). In a critical test of our hypothesis, cell lines were then inoculated with MHV. Somewhat surprisingly, both the TM- and GPI-anchored lines were nearly equivalent in their support of plaque development (Fig. 8A), but plaques expanded to larger sizes on the HeLa-$CEACAM_{TM}$ monolayers. Consistent with this expanded cell-to-cell spread, we found that the activities of $CEACAM_{TM}$ cells were greater than those of $CEACAM_{GPI}$ cells in cell-cell fusion assays (Fig. 8B). Thus, it appeared that, relative to TM anchors, GPI tethers moderately reduced the effectiveness of receptor-triggered cell-cell fusion but had little if any effect on virion binding, uptake, and productive infection. These findings, unlike those reported for HIV (20), argued against the hypothesis that cholesterol augments virus infection by clustering cellular receptors into DRMs.

To further distinguish the requirements for cholesterol during infection of the different HeLa cell lines, we reduced or elevated cholesterol levels prior to MHV inoculation and then monitored plaque development. Our results consistently revealed that, relative to the standard HeLa-$CEACAM_{TM}$ lines, the changing cholesterol levels profoundly altered the susceptibilities of the $CEACAM_{GPI}$ lines (Fig. 8C). This was most pronounced during infections with strain JHM, the most cholesterol-sensitive strain (Fig. 1). Here, CD treatments rendered the $CEACAM_{GPI}$ cells profoundly resistant to infection (nearly 500-fold [Fig. 8C]), whereas infections of $CEACAM_{TM}$ cells were reduced only ~10-fold after the same treatment. Notably, these different cholesterol conditions did not affect virus-cell recognition, as determined by binding of metabolically radiolabeled virions to cells treated with cholesterol or CD (data not shown). Thus, infection through GPI-linked receptors is unusually sensitive to the target lipid environment. This observation may be relevant to coronavirus infection through receptors, such as the proposed GPI-linked brain CEA (15).

Cholesterol extraction blocks S-mediated membrane fusion even in the absence of CEACAM receptors. Our findings suggested that CEACAMs and cholesterol-containing membranes are both required for MHV infection and that colocalization of these two factors augments virus entry. However, it remained unclear whether cholesterol-containing membranes were required in a CEACAM-mediated virus entry process or whether the cholesterol-rich target membranes were directly required for fusion with MHV virion membranes, independent of any activation by CEACAMs. Fortunately, we could determine whether cholesterol is directly required for fusion using variant MHV S proteins that activate spontaneously. Cell-cell fusion mediated by the S proteins from MHV strain JHM can activate spontaneously in the absence of CEACAMs (50, 81), presumably by virtue of their inherent conformational flexibility (42).

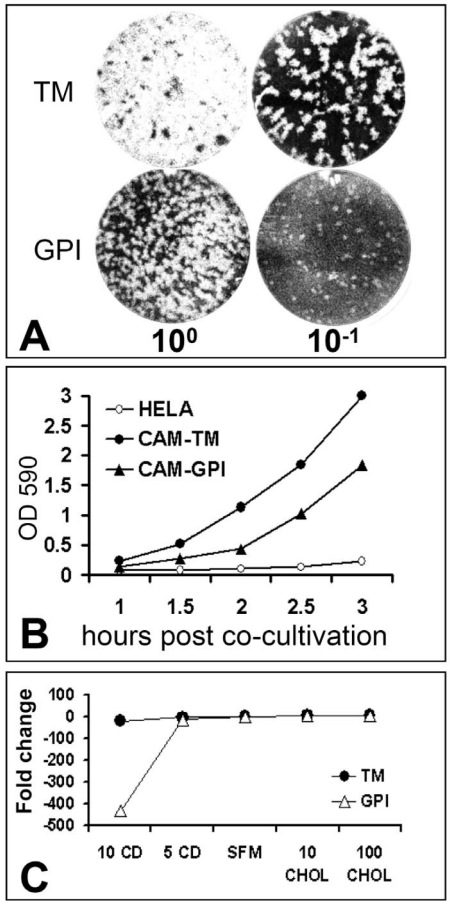

FIG. 8. Susceptibility of HeLa-$CEACAM_{GPI}$ cells to infection and membrane fusion. (A) HeLa-$CEACAM_{TM}$ (TM) and HeLa-$CEACAM_{GPI}$ (GPI) cells were infected with serial 10-fold dilutions of MHV-JHM, and plaques were subsequently visualized. (B) HeLa, HeLa-$CEACAM_{TM}$ (CAM-TM), or HeLa-$CEACAM_{GPI}$ (CAM-GPI) target cells were cocultivated with S-bearing effector cells. At 30-min intervals, the cells in the cocultures were lysed, and cell fusion-activated β-galactosidase enzyme activity in the lysate was quantified by measuring CPRG substrate turnover at an optical density of 590 nm (OD 590). (C) Cells bearing either TM- or GPI-anchored receptors were cultivated in CD (5 or 10 mM) or cholesterol (CHOL) (10 or 100 μg/ml) for 30 min at 37°C. Monolayers were subsequently rinsed, and infectivity was determined by plaque assay. The fold difference in PFU/ml was calculated relative to cells cultured in SFM alone.

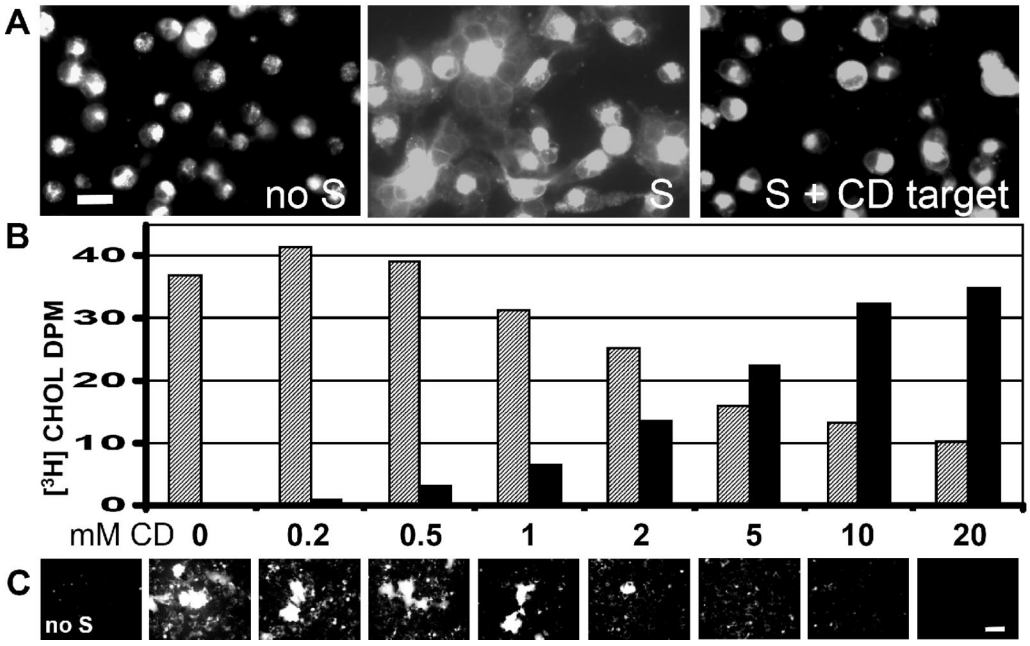

FIG. 9. CEACAM-independent fusion after cholesterol extraction. (A) Photos of R18-labeled target cells 3 h after the cells were cocultivated with unlabeled S-bearing (JHM) effector cells. In the rightmost panel, a parallel culture was treated with 5 mM MβCD for 30 min at 37°C and rinsed prior to cocultivation. Bar, 50 μm. (B) Bar graph showing [^{3}H]cholesterol (CHOL) levels in cells (hatched bars) and media (black bars) after exposure to the indicated millimolar concentrations of MβCD (30 min at 37°C). Cells were previously labeled for 18 h with [^{3}H]cholesterol. After CD treatments, media were removed, cells were lysed, and ^{3}H levels (in disintegrations per minute [DPM]) were determined by scintillation counting. (C) HeLa target cells were treated with Lipofectamine with pTM3-eGFP and then treated with MβCD as described for panel B. Target cells were then overlaid with effector cells presenting S_{JHM}. In this assay, eGFP gene expression is dependent on effector cell-target cell fusion. Micrographs were taken 3 h after cocultivation of effector and target cells. Bar, 100 μm.

cDNAs encoding S_{JHM} were expressed in a variety of nonmurine cell lines, and syncytia developed to highly variable extents. However, in all cell lines tested, foci were more pronounced in parallel cultures that had been pretreated with cholesterol. Conversely, syncytia never formed in cultures exposed to MβCD. These findings were documented by visualizing fusion-dependent reporter gene (eGFP) expression (Fig. 9). In these assays, cholesterol was extracted from target cells with graded doses of MβCD, and the cells were then cocultivated with effector cells expressing the S_{JHM} proteins. The extent of cholesterol extraction achieved by the MβCD treatments was measured in parallel cultures labeled with [^{3}H]cholesterol. Our results indicated that S-mediated membrane fusion was arrested once about 50% of cellular cholesterol was removed from target cells. This block to fusion was achieved entirely by cholesterol extraction of target cell membranes that were devoid of murine CEACAMs, strongly suggesting that cholesterol itself is a fusion cofactor residing in target cell membranes.

DISCUSSION

The in vitro dissemination and in vivo pathogenesis of MHV infections are affected by changing cholesterol concentrations (9). This study was undertaken to explain the underlying mechanisms of this lipid requirement. We quickly determined that the MHV-cell membrane fusion process was specifically inhibited or augmented by cholesterol depletion or supplementation, respectively, placing this coronavirus into a relatively large group of otherwise unrelated viruses whose members include Sindbis virus (46), HIV (31, 49, 62), Ebola virus (6, 23), and more recently herpes simplex virus (7). The cholesterol requirement during virus entry raises the question of whether lipid rafts comprise entry sites, as typical rafts are relatively thick, liquid, ordered bilayers heavily enriched in sphingolipid and cholesterol (12). Therefore, we focused on the MHV receptor CEACAM and its distribution on the plasma membranes of MHV-susceptible cells, anticipating a predominant colocalization with cholesterol-rich rafts. After all, receptors for several cholesterol-dependent viruses appear to reside largely in rafts (5, 41, 62). However, by biochemical subcellular fractionation, we found no compelling evidence for raft-associated CEACAMs. Furthermore, when CEACAMs were engineered with GPI anchors so that they did cluster into rafts, we found no significant change in the susceptibility to infection by virions. Therefore, in our experimental systems, it appears that MHV can enter through traditional detergent-resistant lipid raft microdomains and through nonraft membranes as well. We suggest that specific subcellular receptor localizations provide little advantage to MHV entry, because the natural levels of cholesterol in membranes surrounding both raft and nonraft CEACAMs are sufficient to complete the virus-cell membrane fusion process.

Fate of CEACAM-associated MHVs. When the levels of cholesterol in plasma membrane were reduced in these studies by extraction with MβCD, infections were blocked, and MHV-JHM, a strain exhibiting rapid virus-cell fusion kinetics (42),

was distinctly disadvantaged. In our experiments, virions bound effectively to the CEACAMs on cholesterol-depleted cells, and we allowed these CEACAM-bound particles to remain as endogenous cholesterol synthesis returned cell membranes to homeostasis, a process requiring about 2 h in BHK cell cultures (34). Despite the cholesterol repletion, infection did not occur, suggesting that CEACAM-associated MHV particles had advanced to an irreversibly inactivated state(s) when juxtaposed near cholesterol-depleted target cell membranes. However, this irreversible inactivation was strain specific and most clearly pronounced when the JHM strains were tested (Fig. 1C). We initially assumed that the infection failures that were so prominent with strain JHM resulted from virus "elution," a previously documented temperature-dependent process whereby particles release from CEACAMs, leaving their noncovalently associated, peripheral S1 fragments behind (26). JHM viruses shed into media would be S1 depleted and incompetent for subsequent entry attempts, thus accounting for reduced infectivity (Fig. 1C). However, this hypothesis could not explain the equivalent inactivation of strain JHM-X, which has stable linkages with S1, even when associated with CEACAM receptors at 37°C, and thus does not "elute" (26). Therefore, a more plausible view is that without cholesterol in target membranes, CEACAM-associated virions undergo conformational changes that do not bring about membrane fusion but rather generate a permanently inactive virus structure that eventually denatures or degrades within the host cell or on its surface. Hypersensitivity of JHM strains to cholesterol limitation would thus be explained by their rapid rates of inactivation following CEACAM engagement. The MHV A59 strain, being less responsive to CEACAM binding, presumably can remain infectious long enough to localize near a target membrane whose lipid composition permits fusion. This conceptual framework suggests that different target cell lipid compositions place selection pressure on coronaviruses, creating strains that vary in their threshold and kinetics of CEACAM-induced fusion activation. The JHM strain, selected for growth in the cholesterol-rich central nervous system (85), does exhibit unrestricted S-mediated fusion activity (81). This viewpoint may also shed light on the results of previous studies demonstrating that certain CEACAM-positive tissue cultures can exhibit resistance to the JHM, but not the A59 strain of MHV (87, 88). Such cultures may have cholesterol contents below those required for efficient entry of the JHM strain.

Potential importance of lipid rafts during MHV entry. Our finding that little if any CEACAM copurified with TX-100 DRMs (Fig. 4) must be interpreted with the understanding that lipid rafts are dynamic structures and that CEACAMs may have considerable lateral mobilities in plasma membranes. Thus, it is possible that viruses bound to CEACAMs outside lipid raft microdomains might drift into the cholesterol-rich raft regions suitable for productive membrane fusion or by contrast undergo unproductive and irreversible conformational changes. The cholesterol supplementations that increase susceptibility to infection (Fig. 1) would thus be explained by the relocalization of CEACAMs into lipid rafts (Fig. 5). In the absence of cholesterol supplementation, the majority of virus entry events would be abortive, given the preponderance of CEACAMs outside rafts and the relatively short time that infectivity remains after CEACAM binding. Perhaps this is the case, as the particle-to-PFU ratios for MHV preparations are generally considered to be extraordinarily high, particularly for the JHM strain.

However, retargeting CEACAMs to rafts through GPI anchoring did not enhance viral infectivity or membrane fusion, in striking contrast to analogous studies in which the raft relocalization of CD4 augmented infection by cholesterol-dependent HIV (20). Our measurements of CEACAM-induced MHV fusion revealed that the GPI-anchored CEACAMs were actually inferior activators (Fig. 8B). One explanation for this diminished fusion is that TM spans influence CEACAM ectodomain structures, and hence the activating function, of the binding interaction between CEACAM and S proteins. We do not favor this possibility, as the binding of MHV particles to either GPI- or TM-anchored CEACAMs were indistinguishable (Fig. 6C). Furthermore, entirely soluble forms of the CEACAMs can function to activate S-mediated fusion (81), indicating that membrane anchors are not required in this process. Biophysical considerations lead us to the alternative suggestion that membrane fusion might be suppressed in the raft environment, because there are few fusion-promoting glycerophospholipids in these regions (77). This hypothesis can be addressed with MHV-liposome fusion assays in which target lipid compositions can be readily adjusted. Such assays are planned, but at present our findings with HeLa cells suggest that MHV entry can at least occur in both raft and nonraft environments, making it likely that a narrowly defined target membrane composition is not absolutely required. Indeed, CEACAMs exist in a variety of tissue-specific isoforms (74), likely partitioning variably in vivo into raft-like microdomains, and thus in considering lipid requirements, a relatively lenient membrane fusion activity might be necessary for expansive polytropic coronavirus infections. Our finding that cells with GPI-anchored CEACAMs are more responsive to fluctuations in cellular cholesterol content during MHV infection than TM-anchored CEACAMs (Fig. 8C) suggests that the local lipid environment surrounding CEACAMs can influence infection.

Potential roles for cholesterol during S-mediated fusion. It has been shown that soluble CEACAM receptors can mimic authentic membrane-anchored forms, bind virion S proteins, and induce conformational changes that lead to S-mediated membrane fusion (50). While the nature of these conformational changes is not yet clear, it is known that soluble CEACAM forms bind S1 fragments (43), resulting in changes in the stability of S1-S2 association (42) and alternative S1 oxidation states (45). We assume that additional, perhaps more crucial structural changes must occur in S proteins prior to membrane fusion. To link the virion and cell, a hydrophobic fusion peptide in the integral-membrane S2 chain (47) must intercalate into target membranes. Here there may be a requirement for cholesterol in the target membrane, similar to that observed for the Semliki Forest virus and Sindbis virus alphaviruses (2, 84). Also, this single polypeptide must change its structure in a way that brings virion and cell membranes into close proximity (76). This latter event may have parallels with those of retroviruses and myxoviruses, as there are predicted alpha helical regions, so-called heptad repeats, in membrane-proximal S2 that may collapse into coiled-core cores concomitant with membrane coalescence (8, 75). Cholesterol requirements can also be hypothesized at this stage, as newly formed

pores between bilayers are stabilized by membrane cholesterol (66). In these views, cholesterol would act as a direct entry cofactor and not as an agent that clusters CEACAMs into raft-like microdomains. A direct role for cholesterol was demonstrated during CEACAM-independent membrane fusion (Fig. 9). Furthermore, essential cholesterol molecules exist near CEACAM receptors, but they need not be present in proportion with the sphingolipids required to create what is operationally defined as lipid rafts, namely, TX-100-insoluble membrane bilayers (11). These concepts mirror the results of recent in vitro studies of Semliki forest virus, where its fusion with liposomes did indeed require cholesterol and sphingolipids, but not in the proportions that produced liposome-associated lipid rafts (84). Our findings suggest that lipids such as cholesterol act independently or in cooperation with CEACAMs to promote coronavirus cell entry.

ACKNOWLEDGMENTS

We acknowledge the technical support of Kathleen Larkin and Jeffrey Lenkart. We thank Fumihiro Taguchi (National Institute of Neuroscience, Tokyo, Japan) and Stuart Siddell (University of Wurzburg, Wurzburg, Germany) for antispike monoclonal antibody.

This work was supported in part by Public Health Service grant NS-31616 from the National Institute of Neurological Diseases and Stroke. Edward Thorp was supported by Experimental Immunology training grant AI007508 from the National Institutes of Allergy and Infectious Diseases.

REFERENCES

1. **Acarturk, F., T. Imai, H. Saito, M. Ishikawa, and M. Otagiri.** 1993. Comparative study on inclusion complexation of maltosyl-beta-cyclodextrin, heptakis(2,6-di-O-methyl)-beta-cyclodextrin and beta-cyclodextrin with fucosterol in aqueous and solid state. J. Pharm. Pharmacol. **45:**1028–1032.
2. **Ahn, A., D. L. Gibbons, and M. Kielian.** 2002. The fusion peptide of Semliki forest virus associates with sterol-rich membrane domains. J. Virol. **76:**3267–3275.
3. **Alkhatib, G., C. C. Broder, and E. A. Berger.** 1996. Cell type-specific fusion cofactors determine human immunodeficiency virus type 1 tropism for T-cell lines versus primary macrophages. J. Virol. **70:**5487–5494.
4. **Amundson, D. M., and M. Zhou.** 1999. Fluorometric method for the enzymatic determination of cholesterol. J. Biochem. Biophys. Methods **38:**43–52.
5. **Ashbourne Excoffon, K. J., T. Moninger, and J. Zabner.** 2003. The coxsackie B virus and adenovirus receptor resides in a distinct membrane microdomain. J. Virol. **77:**2559–2567.
6. **Bavari, S., C. M. Bosio, E. Wiegand, G. Ruthel, A. B. Will, T. W. Geisbert, M. Hevey, C. Schmaljohn, A. Schmaljohn, and M. J. Aman.** 2002. Lipid raft microdomains: a gateway for compartmentalized trafficking of Ebola and Marburg viruses. J. Exp. Med. **195:**593–602.
7. **Bender, F. C., J. C. Whitbeck, M. Ponce de Leon, H. Lou, R. J. Eisenberg, and G. H. Cohen.** 2003. Specific association of glycoprotein B with lipid rafts during herpes simplex virus entry. J. Virol. **77:**9542–9552.
8. **Bosch, B. J., R. van der Zee, C. A. de Haan, and P. J. Rottier.** 2003. The coronavirus spike protein is a class I virus fusion protein: structural and functional characterization of the fusion core complex. J. Virol. **77:**8801–8811.
9. **Braunwald, J., H. Nonnenmacher, C. A. Pereira, and A. Kirn.** 1991. Increased susceptibility to mouse hepatitis virus type 3 (MHV3) infection induced by a hypercholesterolaemic diet with increased adsorption of MHV3 to primary hepatocyte cultures. Res. Virol. **142:**5–15.
10. **Brown, D.** 1994. GPI-anchored proteins and detergent-resistant membrane domains. Braz. J. Med. Biol. Res. **27:**309–315.
11. **Brown, D. A., and E. London.** 1998. Functions of lipid rafts in biological membranes. Annu. Rev. Cell Dev. Biol. **14:**111–136.
12. **Brown, D. A., and E. London.** 1997. Structure of detergent-resistant membrane domains: does phase separation occur in biological membranes? Biochem. Biophys. Res. Commun. **240:**1–7.
13. **Cervin, M., and R. Anderson.** 1991. Modulation of coronavirus-mediated cell fusion by homeostatic control of cholesterol and fatty acid metabolism. J. Med. Virol. **35:**142–149.
14. **Chalfie, M., Y. Tu, G. Euskirchen, W. W. Ward, and D. C. Prasher.** 1994. Green fluorescent protein as a marker for gene expression. Science **263:**802–805.
15. **Chen, D. S., M. Asanaka, K. Yokomori, F. Wang, S. B. Hwang, H. P. Li, and M. M. Lai.** 1995. A pregnancy-specific glycoprotein is expressed in the brain and serves as a receptor for mouse hepatitis virus. Proc. Natl. Acad. Sci. USA **92:**12095–12099.
16. **Chernomordik, L.** 1996. Non-bilayer lipids and biological fusion intermediates. Chem. Phys. Lipids **81:**203–213.
17. **Cordy, J. M., I. Hussain, C. Dingwall, N. M. Hooper, and A. J. Turner.** 2003. Exclusively targeting beta-secretase to lipid rafts by GPI-anchor addition up-regulates beta-site processing of the amyloid precursor protein. Proc. Natl. Acad. Sci. USA **100:**11735–11740.
18. **Danieli, T., S. L. Pelletier, Y. I. Henis, and J. M. White.** 1996. Membrane fusion mediated by the influenza virus hemagglutinin requires the concerted action of at least three hemagglutinin trimers. J. Cell Biol. **133:**559–569.
19. **Daya, M., M. Cervin, and R. Anderson.** 1988. Cholesterol enhances mouse hepatitis virus-mediated cell fusion. Virology **163:**276–283.
20. **Del Real, G., S. Jimenez-Baranda, R. A. Lacalle, E. Mira, P. Lucas, C. Gomez-Mouton, A. C. Carrera, A. C. Martinez, and S. Manes.** 2002. Blocking of HIV-1 infection by targeting CD4 to nonraft membrane domains. J. Exp. Med. **196:**293–301.
21. **Dveksler, G. S., C. W. Dieffenbach, C. B. Cardellichio, K. McCuaig, M. N. Pensiero, G.-S. Jiang, N. Beauchemin, and K. V. Holmes.** 1993. Several members of the mouse carcinoembryonic antigen-related glycoprotein family are functional receptors for the coronavirus mouse hepatitis virus-A59. J. Virol. **67:**1–8.
22. **Dveksler, G. S., M. N. Pensiero, C. B. Cardellichio, R. K. Williams, G.-S. Jiang, K. V. Holmes, and C. W. Dieffenbach.** 1991. Cloning of the mouse hepatitis virus (MHV) receptor: expression in human and hamster cell lines confers susceptibility to MHV. J. Virol. **65:**6881–6891.
23. **Empig, C. J., and M. A. Goldsmith.** 2002. Association of the caveola vesicular system with cellular entry by filoviruses. J. Virol. **76:**5266–5270.
24. **Fuerst, T. R., P. L. Earl, and B. Moss.** 1987. Use of a hybrid vaccinia virus-T7 RNA polymerase system for expression of target genes. Mol. Cell. Biol. **7:**2538–2544.
25. **Gallagher, T. M.** 1996. Murine coronavirus membrane fusion is blocked by modification of thiols buried within the spike protein. J. Virol. **70:**4683–4690.
26. **Gallagher, T. M.** 1997. A role for naturally occurring variation of the murine coronavirus spike protein in stabilizing association with the cellular receptor. J. Virol. **71:**3129–3137.
27. **Garcia, R. A., S. P. Pantazatos, D. P. Pantazatos, and R. C. MacDonald.** 2001. Cholesterol stabilizes hemifused phospholipid bilayer vesicles. Biochim. Biophys. Acta **1511:**264–270.
28. **Giurisato, E., D. P. McIntosh, M. Tassi, A. Gamberucci, and A. Benedetti.** 2003. T cell receptor can be recruited to a subset of plasma membrane rafts, independently of cell signaling and attendantly to raft clustering. J. Biol. Chem. **278:**6771–6778.
29. **Gossen, M., and H. Bujard.** 1992. Tight control of gene expression in mammalian cells by tetracycline-responsive promoters. Proc. Natl. Acad. Sci. USA **89:**5547–5551.
30. **Gunther-Ausborn, S., A. Praetor, and T. Stegmann.** 1995. Inhibition of influenza-induced membrane fusion by lysophosphatidylcholine. J. Biol. Chem. **270:**29279–29285.
31. **Guyader, M., E. Kiyokawa, L. Abrami, P. Turelli, and D. Trono.** 2002. Role for human immunodeficiency virus type 1 membrane cholesterol in viral internalization. J. Virol. **76:**10356–10364.
32. **Haque, M. E., T. J. McIntosh, and B. R. Lentz.** 2001. Influence of lipid composition on physical properties and peg-mediated fusion of curved and uncurved model membrane vesicles: "nature's own" fusogenic lipid bilayer. Biochemistry **40:**4340–4348.
33. **Harder, T., P. Scheiffele, P. Verkade, and K. Simons.** 1998. Lipid domain structure of the plasma membrane revealed by patching of membrane components. J. Cell Biol. **141:**929–942.
34. **Heino, S., S. Lusa, P. Somerharju, C. Ehnholm, V. M. Olkkonen, and E. Ikonen.** 2000. Dissecting the role of the Golgi complex and lipid rafts in biosynthetic transport of cholesterol to the cell surface. Proc. Natl. Acad. Sci. USA **97:**8375–8380.
35. **Hirano, N., T. Murakami, K. Fujiwara, and M. Matsumoto.** 1978. Utility of mouse cell line DBT for propagation and assay of mouse hepatitis virus. Jpn. J. Exp. Med. **48:**71–75.
36. **Ho, S. N., H. D. Hunt, R. M. Horton, J. K. Pullen, and L. R. Pease.** 1989. Site-directed mutagenesis by overlap extension using the polymerase chain reaction. Gene **77:**51–59.
37. **Kenworthy, A. K., N. Petranova, and M. Edidin.** 2000. High-resolution FRET microscopy of cholera toxin B-subunit and GPI-anchored proteins in cell plasma membranes. Mol. Biol. Cell **11:**1645–1655.
38. **Kielian, M. C., and A. Helenius.** 1984. Role of cholesterol in fusion of Semliki forest virus with membranes. J. Virol. **52:**281–283.
39. **Kilsdonk, E. P., P. G. Yancey, G. W. Stoudt, F. W. Bangerter, W. J. Johnson, M. C. Phillips, and G. H. Rothblat.** 1995. Cellular cholesterol efflux mediated by cyclodextrins. J. Biol. Chem. **270:**17250–17256.
40. **Klein, U., G. Gimpl, and F. Fahrenholz.** 1995. Alteration of the myometrial plasma membrane cholesterol content with beta-cyclodextrin modulates the binding affinity of the oxytocin receptor. Biochemistry **34:**13784–13793.
41. **Kozak, S. L., J. M. Heard, and D. Kabat.** 2002. Segregation of CD4 and

CXCR4 into distinct lipid microdomains in T lymphocytes suggests a mechanism for membrane destabilization by human immunodeficiency virus. J. Virol. **76:**1802–1815.
42. **Krueger, D. K., S. M. Kelly, D. N. Lewicki, R. Ruffolo, and T. M. Gallagher.** 2001. Variations in disparate regions of the murine coronavirus spike protein impact the initiation of membrane fusion. J. Virol. **75:**2792–2802.
43. **Kubo, H., Y. K. Yamada, and F. Taguchi.** 1994. Localization of neutralizing epitopes and the receptor-binding site within the amino-terminal 330 amino acids of the murine coronavirus spike protein. J. Virol. **68:**5403–5410.
44. **Laemmli, U. K.** 1970. Cleavage of structural proteins during the assembly of the head of bacteriophage T4. Nature **227:**680–685.
45. **Lewicki, D. N., and T. M. Gallagher.** 2002. Quaternary structure of coronavirus spikes in complex with carcinoembryonic antigen-related cell adhesion molecule cellular receptors. J. Biol. Chem. **277:**19727–19734.
46. **Lu, Y. E., T. Cassese, and M. Kielian.** 1999. The cholesterol requirement for Sindbis virus entry and exit and characterization of a spike protein region involved in cholesterol dependence. J. Virol. **73:**4272–4278.
47. **Luo, Z., and S. R. Weiss.** 1998. Roles in cell-to-cell fusion of two conserved hydrophobic regions in the murine coronavirus spike protein. Virology **244:** 483–494.
48. **Makino, S., F. Taguchi, N. Hirano, and K. Fujiwara.** 1984. Analysis of genomic and intracellular viral RNAs of small plaque mutants of mouse hepatitis virus, JHM strain. Virology **139:**138–151.
49. **Manes, S., G. del Real, R. A. Lacalle, P. Lucas, C. Gomez-Mouton, S. Sanchez-Palomino, R. Delgado, J. Alcami, E. Mira, and A. C. Martinez.** 2000. Membrane raft microdomains mediate lateral assemblies required for HIV-1 infection. EMBO Rep. **1:**190–196.
50. **Matsuyama, S., and F. Taguchi.** 2002. Receptor-induced conformational changes of murine coronavirus spike protein. J. Virol. **76:**11819–11826.
51. **Melikyan, G. B., R. M. Markosyan, H. Hemmati, M. K. Delmedico, D. M. Lambert, and F. S. Cohen.** 2000. Evidence that the transition of HIV-1 gp41 into a six-helix bundle, not the bundle configuration, induces membrane fusion. J. Cell Biol. **151:**413–423.
52. **Melkonian, K. A., A. G. Ostermeyer, J. Z. Chen, M. G. Roth, and D. A. Brown.** 1999. Role of lipid modifications in targeting proteins to detergent-resistant membrane rafts. Many raft proteins are acylated, while few are prenylated. J. Biol. Chem. **274:**3910–3917.
53. **Millan, J., M. C. Montoya, D. Sancho, F. Sanchez-Madrid, and M. A. Alonso.** 2002. Lipid rafts mediate biosynthetic transport to the T lymphocyte uropod subdomain and are necessary for uropod integrity and function. Blood **99:**978–984.
54. **Moss, B., O. Elroy-Stein, T. Mizukami, W. A. Alexander, and T. R. Fuerst.** 1990. Product review. New mammalian expression vectors. Nature **348:**91–92.
55. **Navarrete Santos, A., J. Roentsch, E. M. Danielsen, J. Langner, and D. Riemann.** 2000. Aminopeptidase N/CD13 is associated with raft membrane microdomains in monocytes. Biochem. Biophys. Res. Commun. **269:**143–148.
56. **Niethammer, P., M. Delling, V. Sytnyk, A. Dityatev, K. Fukami, and M. Schachner.** 2002. Cosignaling of NCAM via lipid rafts and the FGF receptor is required for neuritogenesis. J. Cell Biol. **157:**521–532.
57. **Nieva, J. L., R. Bron, J. Corver, and J. Wilschut.** 1994. Membrane fusion of Semliki Forest virus requires sphingolipids in the target membrane. EMBO J. **13:**2797–2804.
58. **Nussbaum, O., C. C. Broder, and E. A. Berger.** 1994. Fusogenic mechanisms of enveloped-virus glycoproteins analyzed by a novel recombinant vaccinia virus-based assay quantitating cell fusion-dependent reporter gene activation. J. Virol. **68:**5411–5422.
59. **Ohtani, Y., T. Irie, K. Uekama, K. Fukunaga, and J. Pitha.** 1989. Differential effects of alpha-, beta- and gamma-cyclodextrins on human erythrocytes. Eur. J. Biochem. **186:**17–22.
60. **Ono, A., and E. O. Freed.** 2001. Plasma membrane rafts play a critical role in HIV-1 assembly and release. Proc. Natl. Acad. Sci. USA **98:**13925–13930.
61. **Pelkmans, L., J. Kartenbeck, and A. Helenius.** 2001. Caveolar endocytosis of simian virus 40 reveals a new two-step vesicular-transport pathway to the ER. Nat. Cell Biol. **3:**473–483.
62. **Popik, W., T. M. Alce, and W. C. Au.** 2002. Human immunodeficiency virus type 1 uses lipid raft-colocalized CD4 and chemokine receptors for productive entry into $CD4^+$ T cells. J. Virol. **76:**4709–4722.
63. **Rao, P. V., and T. M. Gallagher.** 1998. Intracellular complexes of viral spike and cellular receptor accumulate during cytopathic murine coronavirus infections. J. Virol. **72:**3278–3288.
64. **Rao, P. V., and T. M. Gallagher.** 1998. Mouse hepatitis virus receptor levels influence virus-induced cytopathology. Adv. Exp. Med. Biol. **440:**549–555.
65. **Rao, P. V., S. Kumari, and T. M. Gallagher.** 1997. Identification of a contiguous 6-residue determinant in the MHV receptor that controls the level of virion binding to cells. Virology **229:**336–348.
66. **Razinkov, V. I., and F. S. Cohen.** 2000. Sterols and sphingolipids strongly affect the growth of fusion pores induced by the hemagglutinin of influenza virus. Biochemistry **39:**13462–13468.
67. **Roos, D. S., C. S. Duchala, C. B. Stephensen, K. V. Holmes, and P. W. Choppin.** 1990. Control of virus-induced cell fusion by host cell lipid composition. Virology **175:**345–357.
68. **Sawicki, S. G.** 1987. Characterization of a small plaque mutant of the A59 strain of mouse hepatitis virus defective in cell fusion. Adv. Exp. Med. Biol. **218:**169–174.
69. **Scheiffele, P., M. G. Roth, and K. Simons.** 1997. Interaction of influenza virus haemagglutinin with sphingolipid-cholesterol membrane domains via its transmembrane domain. EMBO J. **16:**5501–5508.
70. **Schroeder, R. J., S. N. Ahmed, Y. Zhu, E. London, and D. A. Brown.** 1998. Cholesterol and sphingolipid enhance the Triton X-100 insolubility of glycosylphosphatidylinositol-anchored proteins by promoting the formation of detergent-insoluble ordered membrane domains. J. Biol. Chem. **273:**1150–1157.
71. **Screaton, R. A., L. DeMarte, P. Draber, and C. P. Stanners.** 2000. The specificity for the differentiation blocking activity of carcinoembryonic antigen resides in its glycophosphatidyl-inositol anchor. J. Cell Biol. **150:**613–626.
72. **Simons, K., and E. Ikonen.** 1997. Functional rafts in cell membranes. Nature **387:**569–572.
73. **Simons, M., P. Keller, B. De Strooper, K. Beyreuther, C. G. Dotti, and K. Simons.** 1998. Cholesterol depletion inhibits the generation of beta-amyloid in hippocampal neurons. Proc. Natl. Acad. Sci. USA **95:**6460–6464.
74. **Singer, B. B., I. Scheffrahn, R. Heymann, K. Sigmundsson, R. Kammerer, and B. Obrink.** 2002. Carcinoembryonic antigen-related cell adhesion molecule 1 expression and signaling in human, mouse, and rat leukocytes: evidence for replacement of the short cytoplasmic domain isoform by glycosylphosphatidylinositol-linked proteins in human leukocytes. J. Immunol. **168:**5139–5146.
75. **Singh, M., B. Berger, and P. S. Kim.** 1999. LearnCoil-VMF: computational evidence for coiled-coil-like motifs in many viral membrane-fusion proteins. J. Mol. Biol. **290:**1031–1041.
76. **Skehel, J. J., and D. C. Wiley.** 2000. Receptor binding and membrane fusion in virus entry: the influenza hemagglutinin. Annu. Rev. Biochem. **69:**531–569.
77. **Stegmann, T.** 2000. Membrane fusion mechanisms: the influenza hemagglutinin paradigm and its implications for intracellular fusion. Traffic **1:**598–604.
78. **Stuart, A. D., H. E. Eustace, T. A. McKee, and T. D. Brown.** 2002. A novel cell entry pathway for a DAF-using human enterovirus is dependent on lipid rafts. J. Virol. **76:**9307–9322.
79. **Sturman, L. S., C. S. Ricard, and K. V. Holmes.** 1990. Conformational change of the coronavirus peplomer glycoprotein at pH 8.0 and 37°C correlates with virus aggregation and virus-induced cell fusion. J. Virol. **64:**3042–3050.
80. **Sturman, L. S., and K. K. Takemoto.** 1972. Enhanced growth of a murine coronavirus in transformed mouse cells. Infect. Immun. **6:**501–507.
81. **Taguchi, F., and S. Matsuyama.** 2002. Soluble receptor potentiates receptor-independent infection by murine coronavirus. J. Virol. **76:**950–958.
82. **Tooze, J., S. Tooze, and G. Warren.** 1984. Replication of coronavirus MHV-A59 in sac- cells: determination of the first site of budding of progeny virions. Eur. J. Cell Biol. **33:**281–293.
83. **Viard, M., I. Parolini, M. Sargiacomo, K. Fecchi, C. Ramoni, S. Ablan, F. W. Ruscetti, J. M. Wang, and R. Blumenthal.** 2002. Role of cholesterol in human immunodeficiency virus type 1 envelope protein-mediated fusion with host cells. J. Virol. **76:**11584–11595.
84. **Waarts, B. L., R. Bittman, and J. Wilschut.** 2002. Sphingolipid and cholesterol dependence of alphavirus membrane fusion. Lack of correlation with lipid raft formation in target liposomes. J. Biol. Chem. **277:**38141–38147.
85. **Weiner, L. P.** 1973. Pathogenesis of demyelination induced by a mouse hepatitis. Arch. Neurol. **28:**298–303.
86. **White, J., and A. Helenius.** 1980. pH-dependent fusion between the Semliki Forest virus membrane and liposomes. Proc. Natl. Acad. Sci. USA **77:**3273–3277.
87. **Yokomori, K., M. Asanaka, S. A. Stohlman, and M. M. Lai.** 1993. A spike protein-dependent cellular factor other than the viral receptor is required for mouse hepatitis virus entry. Virology **196:**45–56.
88. **Yokomori, K., and M. M. Lai.** 1993. Mouse hepatitis virus infection utilizes more than one receptor and requires an additional cellular factor. Adv. Exp. Med. Biol. **342:**273–277.